Global Mapping of Temperature-Health Risks: A Model of AI for Planetary Health

Junji Cao , Ermo Chen , Peng Chen , Xi Chen , Gang Huang , Gordon G. Liu * , Bernhard Schwartländer , Xiao Tang , Xu Wang , Wanrui Wu , Li Yang

Posted Date: 29 May 2026

doi: 10.20944/preprints202605.2079.v1

Keywords: temperature anomaly; excess mortality; early warning system; SEV decomposition; copula model; climate-health adaptation

 doi:10.20944/preprints202605.2079.v1

Article

Global Mapping of Temperature-Health Risks: A Model of AI for Planetary Health

Junji Cao [1], Ermo Chen [2], Peng Chen [3], Xi Chen [4], Gang Huang [4], Gordon G. Liu [2,*], Bernhard Schwartländer [2], Xiao Tang [1], Xu Wang [3], Wanrui Wu [2] and Li Yang [3]

[1] Institute of Atmospheric Physics, Chinese Academy of Sciences
[2] Institute for Global Health and Development, Peking University
[3] Zhongke Tianji Meteorological Technology Co., Ltd.
[4] State Key Laboratory of Earth System Numerical Modeling and Application, Institute of Atmospheric Physics, Chinese Academy of Sciences
* Correspondence: gordonliu@nsd.pku.edu.cn

Abstract

Temperature anomalies drive substantial excess mortality, yet existing early warning systems remain limited to regional scales, reliant on linear assumptions, and fail to adequately account for multi-dimensional thermal stress and socioeconomic heterogeneity. This study develops the Planetary Health Axis System–Meteorology (PHAS–M), a framework designed to transform sub-daily weather forecasts into location-specific predictions of the risk of temperature-related excess mortality. PHAS-M employs a Bayesian, prior-informed severity–exposure–vulnerability decomposition coupled with a copula model to capture non-linear mechanisms and spatial variation in adaptive capacity. In validation, it dramatically outperforms existing approaches and surpasses both conventional regression and pure machine learning baselines. This methodology further reveals that the heterogeneity of temperature-induced health risks is attributable to socioeconomic vulnerability, and supports the integration of a broader set of heterogeneous characteristics into predictive climate–health models. The PHAS-M framework provides an interpretable and universal operational tool for decision-makers to better intervene in weather-related health risks.

Keywords: temperature anomaly; excess mortality; early warning system; SEV decomposition; copula model; climate-health adaptation

1. Introduction

Temperature anomalies are a primary driver of excess mortality from cardiovascular, respiratory, and metabolic diseases. The association between non-optimal ambient temperature and elevated mortality risk has been well established in the literature, with temperature-sensitive conditions including ischemic heart disease, stroke, chronic obstructive pulmonary disease, and renal failure accounting for a substantial fraction of the global burden of disease attributable to environmental factors (Ballester et al., 2023; Chen et al., 2024; Masselot et al., 2023). Climate change is intensifying the frequency and severity of thermal extremes, with heatwaves intensifying worldwide (Liu et al., 2024; Sun et al., 2024; Luthi et al., 2023; Wang et al., 2025). Accurate temperature-health risk forecasting serves dual public health purposes: it enables healthcare systems to anticipate and prepare for fluctuations in health service demand, including emergency department visits, hospital admissions, and pharmaceutical supply needs (Liao et al., 2025), and it empowers individuals to adopt adaptive behaviors that reduce exposure to extreme temperatures.

Despite the recognized importance of temperature-health risk forecasting, current operational approaches remain relatively preliminary. Two primary methods prevail in practice. The first relies on simple extrapolation based on historical experience, wherein practitioners apply intuitive judgments derived from past temperature-mortality patterns without formal statistical models (Yu

 doi:10.20944/preprints202605.2079.v1

et al., 2024). This approach fails to capture the nonlinear and spatially heterogeneous nature of temperature-health associations and provides limited interpretability and verifiability for decision-making. The second method employs universal parameter estimates, typically expressed as relative risks per degree of temperature departure or threshold-based rules, focusing exclusively on mean temperature or extreme temperature thresholds (Boudreault et al., 2024; Kim & Kim, 2022; Ohashi et al., 2023). More sophisticated approaches, such as time-series quasi-Poisson regression, have been applied regionally (Ballester et al., 2023; Ballester et al., 2024; Garcia-Leon et al., 2024), but typically target specific disease categories with limited forecast horizons, remaining local rather than globally operational.

Furthermore, substantial heterogeneity exists in the temperature-health associations across multiple dimensions, harming the representativeness of uniform parameters across diverse populations and climates. Research has identified significant variation by population characteristics, including age and underlying health conditions (Chen et al., 2024; Falchetta et al., 2024; Tipaldo et al., 2024), by geographic location and climate zone (Gao et al., 2024; Wu et al., 2023; Yuan et al., 2024), and by level of economic development (Li et al., 2024; Mashhoodi & Kasraian, 2024; Masselot et al., 2023). These findings present a fundamental methodological challenge: no matter how large the sample size, developing universal parameter estimates for naive prediction is inherently limited. Therefore, there is a pressing need for a predictive approach that synthesizes global empirical evidence and incorporates multidimensional heterogeneity into a unified model framework, rather than relying on universal parameters or region-specific regression estimates.

This paper addresses this challenge by developing Planetary Health Axis System – Meteorology (PHAS–M), a globally scalable AI framework that transforms sub-daily weather forecasts into location-specific, anomaly-based disease risk scores. We introduce a distilled severity-exposure-vulnerability (SEV) decomposition model to quantify incremental disease burden attributable to forecasted temperature deviations, and we validate its performance against ground-truth incidence data and Global Burden of Disease estimates. The core of our framework separates health risk contributions into three components: severity (temperature stress intensity), exposure (population at risk), and vulnerability (susceptibility modifiers). This structure accommodates heterogeneous effects across populations, geographies, and levels of economic development. Our framework computes 14 temperature indicators from hourly forecast data, capturing not only absolute temperature levels but also intra-day dynamics and variability patterns that influence health outcomes (Alahmad et al., 2023). The final risk score combines these components via a copula-based aggregation that preserves the statistical dependence structure among temperature indicators and captures non-linear interactions that linear models cannot represent.

This study makes three primary contributions to the literature on temperature-health risk research. First, in the empirical analysis, our Shapley decomposition reveals substantial contributions from extreme-anomaly components—including intra-day temperature standard deviation, maximum cooling rate, and diurnal-range percentile—that have been widely neglected in prior work (Alahmad et al., 2023; Boudreault et al., 2023; Liao et al., 2025). Our findings quantitatively confirm that less-popular temperature measures in previous literature can be major sources of explainable variance. Second, by converting sub-daily weather forecasts into location-specific health risk prediction, PHAS–M provides an operational tool to bridge the knowledge-action gap in disease prevention (Falchetta et al., 2024; Xie et al., 2024), enabling consistent, comparable temperature-related health risk predictions across diverse geographic and socioeconomic contexts. Third, we make a methodological contribution by incorporating heterogeneous effects across populations, geographies, and socio-economic characteristics into the framework of temperature-related health risk (Boudreault et al., 2023; Garcia-Leon et al., 2024; Guo et al., 2024).

 doi:10.20944/preprints202605.2079.v1

2. Methods

2.1. Overview of the Framework

The framework operates on a daily cycle for any pre-defined global grid. The workflow comprises four sequential steps that transform raw meteorological forecasts into actionable health risk scores. First, meteorological forecast input: hourly 2-m air temperature forecasts are obtained from the SD3-based numerical weather prediction product and used as the meteorological driver of PHAS-M. Second, anomaly vector construction: for each grid, 14 temperature indicators are computed from the hourly forecast data. Each indicator is expressed as a percentile relative to a 30-year historical baseline for the same calendar day window, producing a standardized anomaly vector that eliminates seasonal confounding.

Third, SEV decomposition risk scoring: the anomaly vector is fed into a distilled severity-exposure-vulnerability decomposition model to yield a grid-level excess mortality risk score that captures non-linear interactions among multiple temperature dimensions.

Fourth, multi-scale aggregation: grid-level scores are aggregated to administrative or ecological zones using population-weighted thresholds, enabling both comparative risk assessment and extreme event flagging for warning generation.

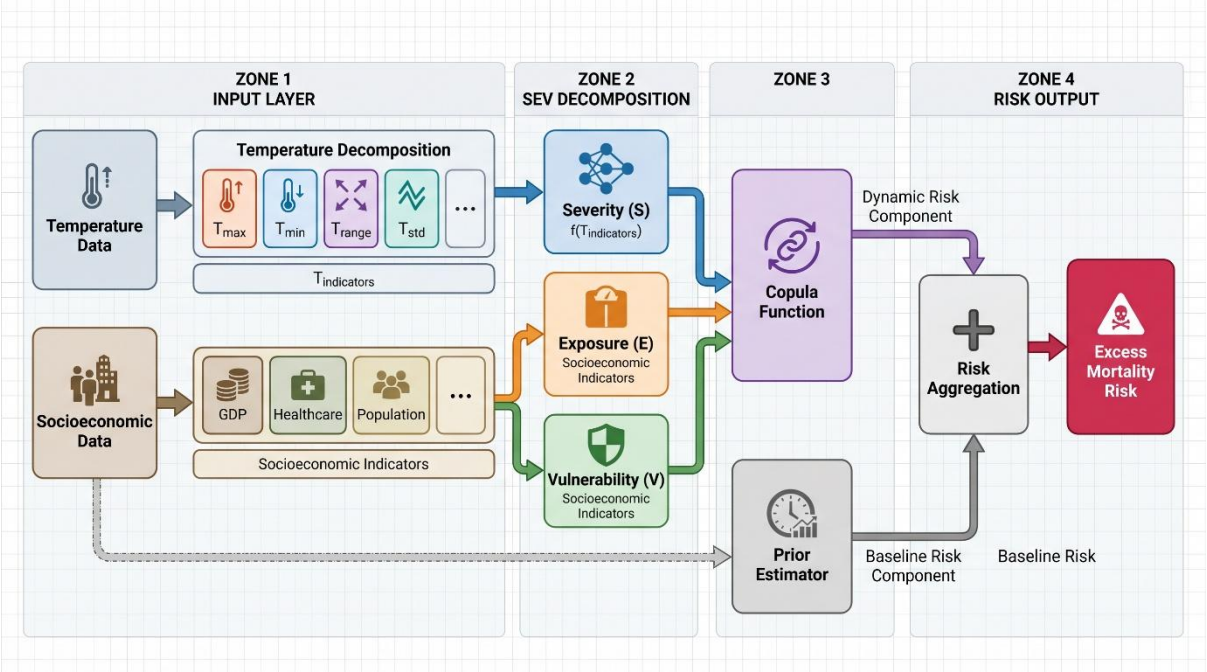

2.2. Meteorological Forecast Input from the SD3 Model.

The meteorological driver of PHAS-M is provided by the SD3-based Tianji numerical weather prediction system. SD3, or Super Dynamics on the Cube, is a non-hydrostatic global modelling system developed from the finite-volume cubed-sphere dynamical core. Previous technical descriptions indicate that SD3 inherits key components of the FV3 dynamical core while introducing improvements in total energy conservation, advection algorithms, vertical remapping, and computational optimization for modern heterogeneous computing systems. The Tianji global-regional integrated numerical weather prediction system is built on a cubed-sphere grid and the SD3 dynamical core, and is designed to support high-resolution global and regional atmospheric simulations.

In this study, we use hourly 2-m air temperature forecasts from the SD3-based forecast product as the meteorological input to PHAS-M. The forecast data used here are prepared on the same horizontal resolution as ERA5, allowing the forecast temperature fields to be directly matched with the historical reference grid used for anomaly calculation. The 2-m air temperature variable

 doi:10.20944/preprints202605.2079.v1

represents near-surface air temperature and is suitable for deriving daily thermal exposure indicators relevant to temperature-related health risks.

For each forecast day, the hourly SD3 temperature sequence is converted into daily meteorological indicators, including daily mean temperature, daily maximum temperature, daily minimum temperature, diurnal temperature range, maximum hourly warming rate, maximum hourly cooling rate, and intra-day temperature standard deviation. These indicators summarize both the absolute thermal state and the intra-day variability of the forecast temperature field. They are subsequently transformed into anomaly features by comparison with historical reference distributions, and the resulting meteorological anomaly vector is used to drive the PHAS-M health-risk prediction model.

High-resolution Tianji forecasts have also been evaluated in impact-oriented hydrometeorological applications, such as extreme rainfall forecasting and hydrological prediction, suggesting their potential value as meteorological inputs for downstream risk-modelling workflows.

2.3. Meteorological Indicators and Anomaly Quantification

For each grid cell and forecast target day, we derive 14 indicators that jointly characterize the predicted temperature abnormalities. This multi-dimensional approach captures not only absolute temperature levels but also intra-day dynamics and variability patterns that have been shown to influence health outcomes. Seven of the 14 indicators capture absolute temperature characteristics, including daily mean temperature (average of 24-hourly readings), daily maximum and minimum temperatures, diurnal temperature range, maximum hourly heating and cooling rates, and intra-day temperature standard deviation. Additionally, we derive the corresponding historical percentiles of the previous 7 indicators to construct the other 7 indicators, computed using a 30-year retrospective baseline with a 7-day moving window centered on the forecast date. This percentile transformation captures the relative departure of each anomaly value from local and seasonal expectations of temperature. Table 1 lists the definition of all temperature indicators.

Table 1. Temperature indicators used in the framework.

Index	Indicator	Definition
W1	Daily mean temperature	Average of 24-hourly readings
W2	Daily maximum temperature	Maximum hourly value
W3	Daily minimum temperature	Minimum hourly value
W4	Diurnal temperature range	W2 minus W3
W5	Maximum hourly heating rate	Max hourly temperature increase
W6	Maximum hourly cooling rate	Max hourly temperature decrease
W7	Intra-day temperature SD	Standard deviation of hourly temps
W8-14	Percentiles of W1-7	Historical percentile position

2.4. Distilled Severity-Exposure-Vulnerability Decomposition Model

The core of the framework is a computationally efficient decomposition model that separates the contributions of severity, exposure, and vulnerability to overall health risk. The risk score is computed through a distilled formulation that separates the contribution of a reduced set of high-priority indicators from a baseline residential estimator derived from offline calibration. This process contains the following steps.

 doi:10.20944/preprints202605.2079.v1

In the first step, each temperature indicator is transformed into a severity score using a sigmoidal activation function to ensure that risks accelerate sharply beyond critical percentile thresholds. The severity function is parameterized by location-specific coefficients that determine the response threshold and steepness. This helps the model understand that the same temperature indicator might have different health-severity effects across different locations.

Second, exposure weights are assigned based on static grid-level population counts and age-standardized disease prevalence. These weights reflect the underlying population at risk for temperature-sensitive health outcomes. With this step, areas with smaller populations will not significantly confuse the model's training.

Lastly, vulnerability coefficients capture spatial variation, containing baseline disease susceptibility, adaptive capacity, and health system resilience. These coefficients are derived from an interpretable approximation of the full PHAS (Planetary Health Axis System) model, used to characterize the impact of various natural, social, and behavioral factors on excess mortality from temperature-sensitive diseases.

The final risk score combines these three components through a copula-based aggregation that preserves the statistical dependence structure among temperature indicators, see Equation (1),

$$\widetilde{\rho_t^{(\alpha)}} = \mathrm{k}g\left(\left[\sum_{i=1}^{N'}\sum_{j=1}^{N'}\left(S_{i,t}^{(\alpha)}E_i^{(\alpha)}V_i^{(\alpha)}\right)^{\gamma'}\left(S_{j,t}^{(\alpha)}E_j^{(\alpha)}V_j^{(\alpha)}\right)^{\gamma'}C'(i,j)\right]^{1/\gamma'} + \widehat{\rho_t^{(\alpha)}}\right). \quad (1)$$

where $\widetilde{\rho_t^{(\alpha)}}$ represents the PHAS-M risk at time t at location α, N' represents the weather indicators considered by PHAS-M, γ', C' represents the modified Copula parameters, $\widehat{\rho_t^{(\alpha)}}$ for residential estimator of the risk at time t at location α by PHAS, k for Overall scale modifier and $g(\cdot)$ for a monotonically transform mapping. An overall scale factor calibrates the output to mortality units.

3. Results

3.1. Model Performance

We evaluated PHAS-M against four comparative approaches: standard excess death ratio predictor for specific diseases in published papers (Alahmad et al., 2024; Chen et al., 2026; Huang et al., 2025; Tobias et al., 2026), a weather-abnormal regression model, a plain machine learning model using all input variables that PHAS-M uses, and a plain machine learning model using weather anomaly features.

Figure 1 presents the out-of-sample root-mean-square error (RMSE) for each model across three diseases. Compared with conventional methods that rely on published baseline coefficients or traditional regression techniques, PHAS-M achieved substantially lower prediction errors, with RMSE reductions ranging from 1.2-fold to 15.1-fold depending on the disease type.

Notably, for stroke prediction, the standard predictor yielded an RMSE of 52.740, which PHAS-M reduced to 3.487, which is a 15-fold improvement that underscores the limitations of applying generic, non-contextualized coefficients to region-specific health forecasting. Also, for lower respiratory infection, PHAS-M achieved an RMSE of 2.107 compared with 20.844 for the standard predictor and 19.584 for the weather-abnormal regression model. For heat stroke, where baseline performance was relatively stronger, PHAS-M still achieved the error at 2.625. These findings indicate that theoretically driven, context-specific modeling substantially outperforms approaches that assume point-to-point uniform temperature-health relationships across populations.

Furthermore, the comparison between machine learning models with and without socioeconomic variables provides compelling evidence for the moderating role of contextual factors in temperature-health associations. When socioeconomic variables were excluded from the prediction model, RMSE values increased dramatically, suggesting that the health effects of future

 doi:10.20944/preprints202605.2079.v1

temperature variations are not determined solely by temperature but are significantly modulated by underlying socioeconomic conditions.

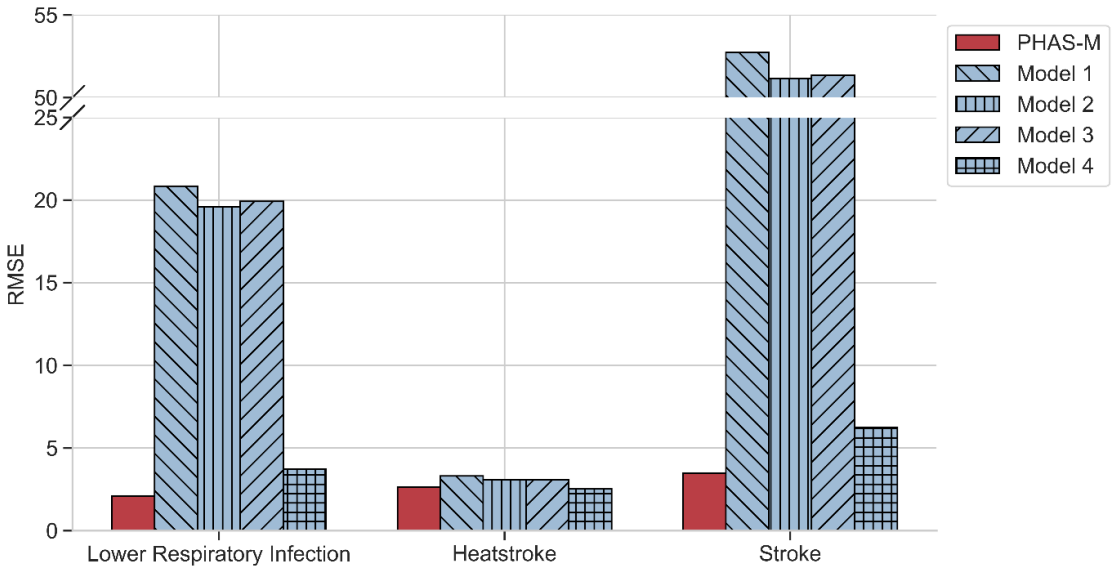

Figure 1. RMSE comparison across five models and three diseases. PHAS-M (red) consistently outperforms all baseline approaches, with particularly large gains for lower respiratory infection and stroke. Model 1 represents the standard excess death ratio predictor. Model 2 is the general generalized linear model. Model 3 is a fully machine learning model using meteorological indicators only, and Model 4 extents Model 3 using all the data same with PHAS-M.

The superior performance of PHAS-M over the Model 3 and Model 4 (RMSE reductions of 43.5% for LRI and 44.2% for stroke) further confirms that theory-guided model specification, which explicitly accounts for effect heterogeneity across regions and populations, yields more accurate predictions than purely data-driven empirical approaches. These results collectively validate the PHAS-M framework as a robust tool for capturing the complex, multidimensional nature of short-term temperature-related health effects, enabling more precise and reliable estimates for public health planning and climate adaptation strategies.

3.2. Country-Level Severity-Vulnerability Risk Stratification

Figure 2 presents country-level scatter plots of severity rank against vulnerability rank for each disease. Severity captures the mean magnitude of temperature anomalies experienced by each country, while vulnerability reflects the mean level of fragile on temperature anomalies for specific diseases, determined by all the socioeconomic factors. The plots are divided into four quadrants by median values and with rank axe, creating a risk classification framework.

The first quadrant is the region where both severity and vulnerability are high; the second quadrant is the region where severity is high but vulnerability is low; the third quadrant is the region where both severity and vulnerability are low; and the fourth quadrant is the region where severity is low but vulnerability is high.

 doi:10.20944/preprints202605.2079.v1

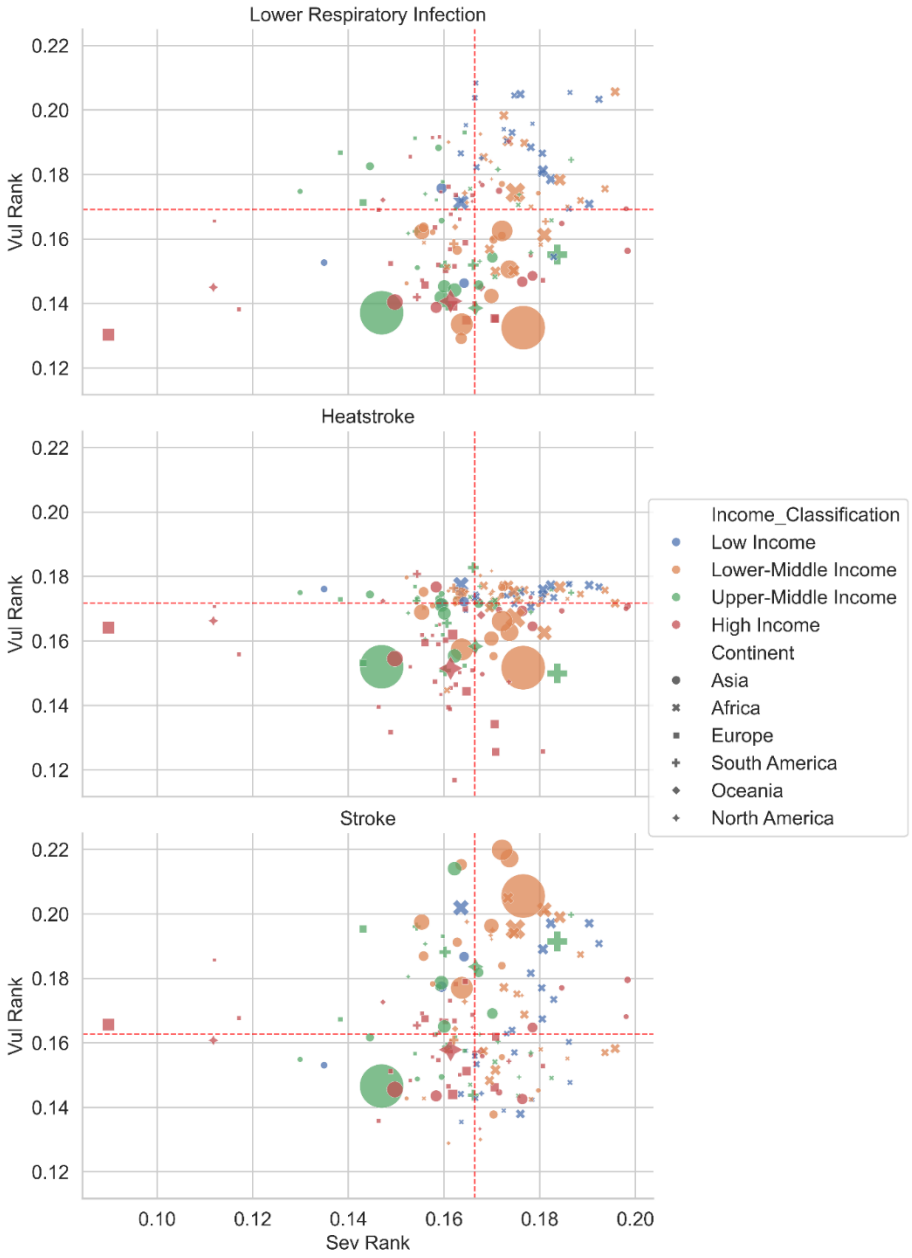

Figure 2. Country-level severity-vulnerability scatter plots for lower respiratory infection (left), heat stroke (center), and stroke (right). Each point represents a country. Points in the upper-right quadrant face compounding high severity and high vulnerability.

For lower respiratory infection, sub-Saharan African nations concentrate heavily in the upper-right quadrant, facing both severe temperature anomalies and high baseline vulnerability driven by limited health infrastructure and high underlying disease prevalence. This compounding effect identifies a population at particularly elevated risk where temperature deviations may trigger substantial excess mortality.

For heat stroke, the pattern is more dispersed. Some countries with relatively mild temperature anomalies exhibit high vulnerability due to low adaptive capacity, while others experience severe anomalies but benefit from stronger health systems. This decoupling of severity and vulnerability underscores the importance of considering both dimensions rather than relying on exposure alone.

For stroke, populous developing nations including Pakistan, Bangladesh, India, and Brazil cluster densely in the upper-right quadrant. These countries combine large exposed populations,

 doi:10.20944/preprints202605.2079.v1

substantial temperature anomaly severity, and significant baseline cerebrovascular disease burden with health systems that may be overwhelmed by surge events.

3.3. Socioeconomic Drivers of Vulnerability

Figure 3 presents bubble charts showing the contribution of selected 17 socioeconomic indicators (not all, but representative) to vulnerability across seven weather indices for each disease. Bubble size represents the magnitude of contribution, revealing which socioeconomic factors most strongly modify temperature-health risk.

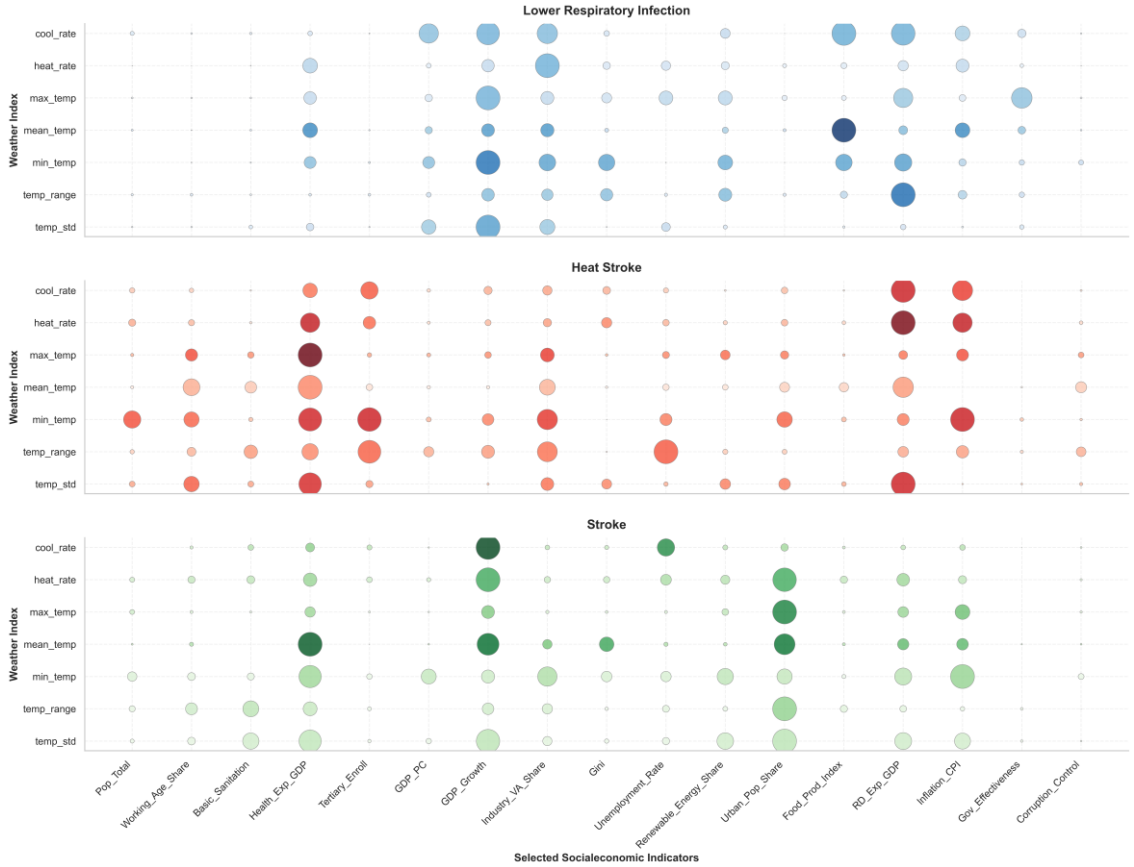

Figure 3. Socioeconomic contribution to vulnerability across diseases and weather dimensions. Bubble size represents contribution magnitude.

Figure 3 demonstrate that vulnerability to weather-related health risks is not uniformly distributed across socioeconomic dimensions. Distinct patterns emerge that vary considerably by both the underlying weather exposure metric and the specific disease outcome under consideration.

From a universal perspective, the GDP growth rate, the share of health expenditure, the share of industrial GDP, the urbanization rate, the share of R&D expenditure, and the inflation rate exert relatively strong influences on vulnerability. In contrast, factors such as population, employment rate, Gini coefficient, government effectiveness, and control of corruption generally have weaker effects. Basic health infrastructure, educational attainment, and food production contribute significantly only to vulnerability to specific diseases.

For lower respiratory infection, prominent contributions observed under the GDP growth rate, Food production, and the share of R&D expenditure. The strong interaction between food production capacity and temperature metrics suggests that nutritional status, itself a function of agricultural productivity, modifies susceptibility to respiratory infections in thermally stressed environments. The GDP growth rate variable demonstrates widespread effect modification, indicating that

 doi:10.20944/preprints202605.2079.v1

economic dynamism may enhance population resilience through improved housing quality, reduced crowding, and better access to healthcare services. Research has consistently demonstrated that respiratory infection burden is concentrated among economically disadvantaged populations, and these findings underscore the role of macroeconomic conditions in shaping differential vulnerability.

The heat stroke panel demonstrates the most extensive pattern of effect modification, with particularly large bubbles observed under the share of healthcare expenditure, the share of R&D expenditure, Education level, and the inflation rate. These findings suggest that heat-related mortality and morbidity are strongly conditioned by a nation's capacity to invest in health infrastructure, its level of technological and educational development, and macroeconomic stability. The pervasive influence of the share of healthcare expenditure across virtually all the weather indices implies that healthcare system capacity serves as a critical buffer against heat-related health crises. Additionally, the significant contributions of tertiary education enrollment suggest that human capital development may enhance community-level awareness and individual behavioral adaptations to extreme heat events.

For stroke, the most substantial bubbles concentrated under the GDP growth rate and the urbanization rate, alongside notable contributions from the share of healthcare expenditure. The strong urban population share effect suggests that rapid urbanization processes may introduce cardiovascular vulnerabilities through mechanisms including air pollution exposure, sedentary lifestyle patterns, and altered dietary transitions. The prominence of the GDP growth rate in effect modification aligns with literature documenting the epidemiological transition in cardiovascular risk profiles during periods of economic development. These findings indicate that stroke vulnerability in the context of temperature extremes is substantially conditioned by urbanization dynamics and economic development trajectories.

The findings presented in Figure 3 carry significant implications for targeted intervention design. The differential patterns across diseases suggest that adaptation strategies should be disease-specific. Also, the consistent importance of health expenditure across all outcomes reinforces the imperative for sustained investment in healthcare infrastructure as a cornerstone of climate-health adaptation. Furthermore, the strong urban population share effects for stroke indicate that urban planning and the management of urbanization processes represent critical levers for reducing cardiovascular vulnerability to temperature extremes.

4. Discussion

4.1. Non-Linear Physiological and Epidemiological Foundations

The superiority of PHAS-M over alternatives is underpinned by well-documented non-linear physiological responses to thermal stress, effected by complex natural and socioeconomical environments. For example, human thermoregulation exhibits threshold-dependent activation of sympathetic nervous and renin-angiotensin systems, with cardiovascular strain increasing disproportionately beyond individual-specific temperature bounds. Similarly, rapid cooling rates have been shown to trigger bronchoconstriction and elevate blood viscosity, mechanisms that are poorly captured by daily mean temperatures alone. The inclusion of intra-day variability and hourly change rates therefore aligns with physiological evidence, while the percentile transformation accommodates acclimatization and local adaptation.

The vulnerability components address a fundamental source of confounding in global studies, where the same absolute temperature anomaly may produce negligible health impacts in a high-income, well-insulated urban center yet catastrophic excess mortality in a low-income, informally housed community. By explicitly modelling this spatial heterogeneity, the PHAS-M framework avoids the ecological fallacy inherent in regionally pooled exposure-response functions.

4.2. Science-Based Support for Resilience Decision-Making

PHAS-M simultaneously provides three key functions.

 doi:10.20944/preprints202605.2079.v1

First, the framework furnishes policymakers with actionable early warning intelligence that identifies both the geographic loci and anticipated severity of impending health risks, thereby extending the temporal window available for loss mitigation. By translating meteorological forecasts and socioeconomic baselines into probabilistic mortality projections, the system enables advance deployment of medical resources, preemptive activation of emergency response protocols, and targeted public health advisories before hazardous weather events materialize. This expanded lead time transforms reactive crisis management into anticipatory governance, reducing both the human toll and the economic burden of climate-sensitive disease outbreaks.

Second, the model delivers a globally comprehensive, nonlinear, and mechanistically grounded risk-science analysis of meteorological health impacts. Rather than relying upon simple linear exposure-response associations, it employs a prior-informed Severity-Exposure-Vulnerability decomposition coupled with copula-based dependence modeling to disaggregate weather-related excess mortality across administrative regions and disease categories. By explicitly partitioning these three drivers, the framework furnishes a more robust epistemic foundation for risk attribution than conventional aggregate models, thereby clarifying whether observed mortality elevations stem primarily from extreme weather intensification, demographic concentration in hazard zones, or systemic deficits in adaptive capacity.

Third, the system generates three integrated lookup dictionaries that translate complex risk decompositions into directly actionable policy intelligence. Policymakers may query the first dictionary to identify, within their specific jurisdiction, which disease category accounts for the greatest burden of excess mortality under projected climate trajectories. The second dictionary reveals which meteorological anomaly serves as the dominant proximate driver of that disease-specific mortality surplus. The third dictionary isolates the socioeconomic or infrastructural factor most vulnerable to that anomaly, such as aged residential density, healthcare accessibility deficits, or energy poverty. Armed with this triangulated diagnostic profile, authorities can design precisely targeted interventions that address the specific causal nexus responsible for elevated mortality risk in their population, rather than dispersing resources across generically defined preparedness measures.

These three functions enable decision-makers to formulate region- and disease-specific intervention policies in a scientifically sound, agile, and robust manner, thereby integrating actionable risk science directly into resilience decision-making.

4.3. Limitations and Future Work

Several limitations warrant mention. The current specification relies exclusively on temperature as the meteorological driver and has yet to incorporate humidity, air pollution, or wind speed, all of which may independently modify heat and cold stress, so a multi-hazard extension is under active development. The vulnerability atlas remains static, reflecting two deliberate analytical boundaries of the present framework. One is that it targets the near future, specifically within a two-week horizon, and the other is that it estimates contemporaneous rather than long-run mortality effects, thereby abstracting from the temporal evolution of socioeconomic adaptive capacity. Future iterations should relax both constraints to accommodate dynamically updating vulnerability profiles. Finally, the distilled model parameters require periodic recalibration as climate baselines shift and dynamic emerge in the temperature-mortality relationship.

5. Conclusions

In summary, this paper develops a predictive model for excess mortality risk induced by meteorological anomalies, grounded in risk theory, and quantifies the impact of temperature anomalies on specific diseases at the global scale. Within a Bayesian framework, the model decomposes the excess mortality risk attributable to meteorological anomalies along each anomaly dimension into three components—severity, exposure, and vulnerability—and links them via a copula function. This architecture effectively integrates the predictive accuracy of atmospheric

 doi:10.20944/preprints202605.2079.v1

models in short-term meteorological anomaly forecasting with the strengths of PHAS in elucidating climate anomaly-induced disease burden, thereby forming a global-scale meteorological health risk governance tool that is simultaneously precise, interpretable, and actionable. With the support of this instrument, jurisdictions worldwide can execute meteorological health risk prevention and control with genuine foresight, precision, and scientific rigor.

Acknowledgments: We thank the Planetary Health Axis System, Peking University for providing the foundational model, the Institute of Atmospheric Physics, Chinese Academy of Sciences for providing meteorological forecasts, and Zhongke Tianji Meteorological Technology Co., Ltd. for providing engineering infrastructure.

References

1. Alahmad, B., Khraishah, H., Kamineni, M., Royé, D., Papatheodorou, S. I., Vicedo-Cabrera, A. M., Guo, Y., Lavigne, E., Armstrong, B., Sera, F., Bernstein, A. S., Zanobetti, A., Garshick, E., Schwartz, J., Bell, M. L., Al-Mulla, F., Koutrakis, P., Gasparrini, A., & Multi-Country Multi-City, N. Extreme temperatures and stroke mortality: evidence from a multi-country analysis. Stroke,2024,55(7), 1847-1856.
2. Alahmad, B., Khraishah, H., Roye, D., Vicedo-Cabrera, A. M., Guo, Y., Papatheodorou, S. I., Achilleos, S., Acquaotta, F., Armstrong, B., Bell, M. L., Pan, S.-C., Zanotti Stagliorio Coelho, M. de S., Colistro, V., Dang, T. N., Van Dung, D., De Donato, F. K., Entezari, A., Guo, Y.-L. L., Hashizume, M., Honda, Y., Indermitte, E., Iniguez, C., Jaakkola, J. J. K., Kim, H., Lavigne, E., Lee, W., Li, S., Madureira, J., Mayvaneh, F., Orru, H., Overcenco, A., Ragettli, M. S., Ryti, N. R. I., Saldiva, P. H. N., Scortichini, N., Seposo, X., Sera, F., Silva, S. P., Stafoggia, M., Tobias, A., Garshick, E., Bernstein, A. S., Zanobetti, A., Schwartz, J., Gasparrini, A., & Koutrakis, P. (2023). Associations between extreme temperatures and cardiovascular cause-specific mortality: Results from 27 countries. Circulation, 147(1), 35–46.
3. Ballester, J., Quijal-Zamorano, M., Turrubiates, R. F. M., Pegenaute, F., Herrmann, F. R., Robine, J. M., Basagana, X., Tonne, C., Anto, J. M., & Achebak, H. (2023). Heat-related mortality in Europe during the summer of 2022. Nature Medicine, 29(7), 1857–1866.
4. Ballester J., Beas-Moix M., Beltrán-Barrón N., Chen Z. Y., Méndez Turrubiates R. F., Peyrusse F., Quijal-Zamorano M. (2024). Forecaster.Health. Available at https://forecaster.health/
5. Boudreault, J., Campagna, C., & Chebana, F. (2023). Machine and deep learning for modelling heat-health relationships. Science of the Total Environment, 892, 164660.
6. Boudreault, J., Campagna, C., & Chebana, F. (2024). Revisiting the importance of temperature, weather and air pollution variables in heat-mortality relationships with machine learning. Environmental Science and Pollution Research, 31(9), 14059–14070.
7. Chen, C., Schwarz, L., Rosenthal, N., Marlier, M. E., & Benmarhnia, T. (2024). Exploring spatial heterogeneity in synergistic effects of compound climate hazards: Extreme heat and wildfire smoke on cardiorespiratory hospitalizations in California. Science Advances, 10(5), eadj7264.
8. Chen, E., Kickbusch, I., Liu, G. G., Lotze-Campen, H., Schwartländer, B., & Wong, B. L. H. (2026). Path to Planetary Health: Call for Three Transformative Shifts Enabled by AI. In (Manuscript in preparation ed.).
9. Chen, K., de Schrijver, E., Sivaraj, S., Sera, F., Scovronick, N., Jiang, L., Roye, D., Lavigne, E., Kysely, J., Urban, A., Schneider, A., Huber, V., Madureira, J., Mistry, M. N., Cvijanovic, I., Gasparrini, A., Vicedo-Cabrera, A. M., Correa, P. M., & Ortega, N. V. (2024). Impact of population aging on future temperature-related mortality at different global warming levels. Nature Communications, 15(1), 1796.
10. Falchetta, G., De Cian, E., Wing, I. S., & Carr, D. (2024). Global projections of heat exposure of older adults. Nature Communications, 15(1), 3678.
11. Gao, S., Chen, Y., Chen, D., He, B., Gong, A., Hou, P., Li, K., & Cui, Y. (2024). Urbanization-induced warming amplifies population exposure to compound heatwaves but narrows exposure inequality between global North and South cities. npj Climate and Atmospheric Science, 7(1), 154.
12. Garcia-Leon, D., Masselot, P., Mistry, M. N., Gasparrini, A., Motta, C., Feyen, L., & Ciscar, J.-C. (2024). Temperature-related mortality burden and projected change in 1368 European regions: A modelling study. Lancet Public Health, 9(9), e644–e653.

 doi:10.20944/preprints202605.2079.v1

13. Guo, F., Zheng, R., Zhao, J., Zhang, H., & Dong, J. (2024). Framework of street grid-based urban heat vulnerability assessment: Integrating entropy weight method and BPNN model. Urban Climate, 56, 102067.
14. He, C., Breitner, S., Zhang, S., Huber, V., Naumann, M., Traidl-Hoffmann, C., Hammel, G., Peters, A., Ertl, M., & Schneider, A. (2024). Nocturnal heat exposure and stroke risk. European Heart Journal, 45(24), 2158–2166.
15. Hersbach, H., Bell, B., Berrisford, P., Hirahara, S., Horányi, A., Muñoz-Sabater, J., Nicolas, J., Peubey, C., Radu, R., Schepers, D., Simmons, A., Soci, C., Abdalla, S., Abellan, X., Balsamo, G., Bechtold, P., Biavati, G., Bidlot, J., Bonavita, M., ... Thépaut, J.-N. (2020). The ERA5 global reanalysis. Quarterly Journal of the Royal Meteorological Society, 146(730), 1999–2049.
16. Huang, W., Yin, L., Li, H., Yang, W., Huang, S., Wang, L., Wang, K., Hao, Y., Wu, Q., & Liu, H. Impact of temperature variations on burden of lower respiratory infections under climate change (1990–2021). BMC Public Health,2025,25(1), 1972.
17. Kim, Y., & Kim, Y. (2022). Explainable heat-related mortality with random forest and SHapley Additive exPlanations (SHAP) models. Sustainable Cities and Society, 79, 103677.
18. Li, F., Yigitcanlar, T., Nepal, M., Nguyen, K., Dur, F., & Li, W. (2024). Assessing heat vulnerability and multidimensional inequity: Lessons from indexing the performance of Australian capital cities. Sustainable Cities and Society, 115, 105875.
19. Li, W.-t., Zhang, J.-p., Sun, R.-c., & Duan, Q. (2023). Evaluation of Tianji and ECMWF high-resolution precipitation forecasts for extreme rainfall event in Henan in July 2021. Water Science and Engineering, 16(2), 122–131.
20. Liao, S., Pan, W., Wen, L., Chen, R., Pan, D., Wang, R., Hu, C., Duan, H., Weng, H., Tian, C., Kong, W., Ruan, J., Zhang, Y., Ming, X., Zhang, X., Wang, X. (2025). Temperature-related hospitalization burden under climate change. Nature, 644(8078), 960–969.
21. Liu, J., Qi, J., Yin, P., Liu, W., He, C., Gao, Y., Zhou, L., Zhu, Y., Kan, H., Chen, R., & Zhou, M. (2024). Rising cause-specific mortality risk and burden of compound heatwaves amid climate change. Nature Climate Change, 14(11), 1027–1035.
22. Luthi, S., Fairless, C., Fischer, E. M., Scovronick, N., Coelho, M. de S. Z. S., Guo, Y. L., Guo, Y., Honda, Y., Huber, V., Kysely, J., Lavigne, E., Roye, D., Ryti, N., Silva, S., Urban, A., Gasparrini, A., Bresch, D. N., & Vicedo-Cabrera, A. M. (2023). Rapid increase in the risk of heat-related mortality. Nature Communications, 14(1), 4894.
23. Masselot, P., Mistry, M., Vanoli, J., Schneider, R., Iungman, T., Garcia-Leon, D., Ciscar, J.-C., Feyen, L., Orru, H., Urban, A., Breitner, S., Huber, V., Schneider, A., Samoli, E., Stafoggia, M., de Donato, F., Rao, S., Armstrong, B., Nieuwenhuijsen, M., Vicedo-Cabrera, A. M., Gasparrini, A., Achilleos, S., Kysely, J., Indermitte, E., Jaakkola, J. J. K., Ryti, N., Pascal, M., Analitis, A., Katsouyanni, K., Goodman, P., Zeka, A., Michelozzi, P., Houthuijs, D., Ameling, C., Pereira da Silva, S., Madureira, J., Holobaca, I.-H., Tobias, A., Iniguez, C., Forsberg, B., Ragettli, M. S., Zafeiratou, S., Fernandez, L. V., Monteiro, A., Rai, M., Zhang, S., & Aunan, K. (2023). Excess mortality attributed to heat and cold: A health impact assessment study in 854 cities in Europe. Lancet Planetary Health, 7(4), e271–e281.
24. Mashhoodi, B., & Kasraian, D. (2024). Heatwave exposure inequality: An urban-rural comparison of environmental justice. Applied Geography, 164, 103216.
25. Ohashi, Y., Ihara, T., Oka, K., Takane, Y., & Kikegawa, Y. (2023). Machine learning analysis and risk prediction of weather-sensitive mortality related to cardiovascular disease during summer in Tokyo, Japan. Scientific Reports, 13(1), 17020.
26. Sun, Y., Zhu, S., Wang, D., Duan, J., Lu, H., Yin, H., Tan, C., Zhang, L., Zhao, M., Cai, W., Wang, Y., Hu, Y., Tao, S., & Guan, D. (2024). Global supply chains amplify economic costs of future extreme heat risk. Nature, 627(8005), 785–790.
27. Tipaldo, J. F., Balk, D., & Hunter, L. M. (2024). A framework for ageing and health vulnerabilities in a changing climate. Nature Climate Change, 14(11), 1125–1135.
28. Tobias, A., Honda, Y., Madaniyazi, L., Alahmad, B., Lavigne, E., Roye, D., Tong, S., de Sousa Zanotti Stagliorio Coelho, M., Huber, V., Urban, A., das Neves Pereira da Silva, S., Achilleos, S., Parks, R. M., Iniguez, C., Masselot, P., Vicedo-Cabrera, A. M., Armstrong, B., Gasparrini, A., Hashizume, M., & Multi-

 doi:10.20944/preprints202605.2079.v1

City Multi-Country Collaborative Research, N. Variation in reporting of heatstroke mortality: evidence from a multi-country study. The Lancet Public Health,2026,11(3), e156-e163.

29. Wang, S., Zhan, W., Zhou, B., Tong, S., Chakraborty, T. C., Wang, Z., Huang, K., Du, H., Middel, A., Li, J., Liu, Z., Li, L., Huang, F., & Li, M. (2025). Dual impact of global urban overheating on mortality. Nature Climate Change, 15(5), 497–506.
30. Wu, S., Yu, W., & Chen, B. (2023). Observed inequality in thermal comfort exposure and its multifaceted associations with greenspace in United States cities. Landscape and Urban Planning, 233, 104701.
31. Xian, Z., Zhu, J., Lin, S.-J., Liang, Z., Chen, X., & Chen, K. (2024). Impact of assimilating Geostationary Interferometric Infrared Sounder observations from long- and middle-wave bands on weather forecasts with a locally cloud-resolving global model. Remote Sensing, 16(18), 3458.
32. Xie, Y., Zhou, Z., Sun, Q., Zhao, M., Pu, J., Li, Q., Sun, Y., Dai, H., & Li, T. (2024). Social-economic transitions and vulnerability to extreme temperature events from 1960 to 2020 in Chinese cities. iScience, 27(3), 109066.
33. Yu, Y., Hossain, M. M., Sikder, R., Qi, Z., Huo, L., Chen, R., Dou, W., Shi, B., & Ye, T. (2024). Exploring the potential of machine learning to understand the occurrence and health risks of haloacetic acids in a drinking water distribution system. Science of the Total Environment, 951, 175573.
34. Yuan, Y., Li, X., Wang, H., Geng, X., Gu, J., Fan, Z., Wang, X., & Liao, C. (2024). Unraveling the global economic and mortality effects of rising urban heat island intensity. Sustainable Cities and Society, 116, 105902.